UCRL-JC-131590
Preprint

A Finite-Difference Frequency-Domain Code for Electromagnetic Induction Tomography

N. J. Campagne II, J. G. Berryman, H. M. Buettner,
J. B. Grant, R. M. Sharpe

This paper was prepared for submittal to
Symoposium of the Application of Geophysics to Engineering and Environment Problems
Proceedings of the Environmental and Engineering Geophysical Society
Oakland Marriott Center, Oakland, CA.
March 14-18, 1999

December 17, 1998

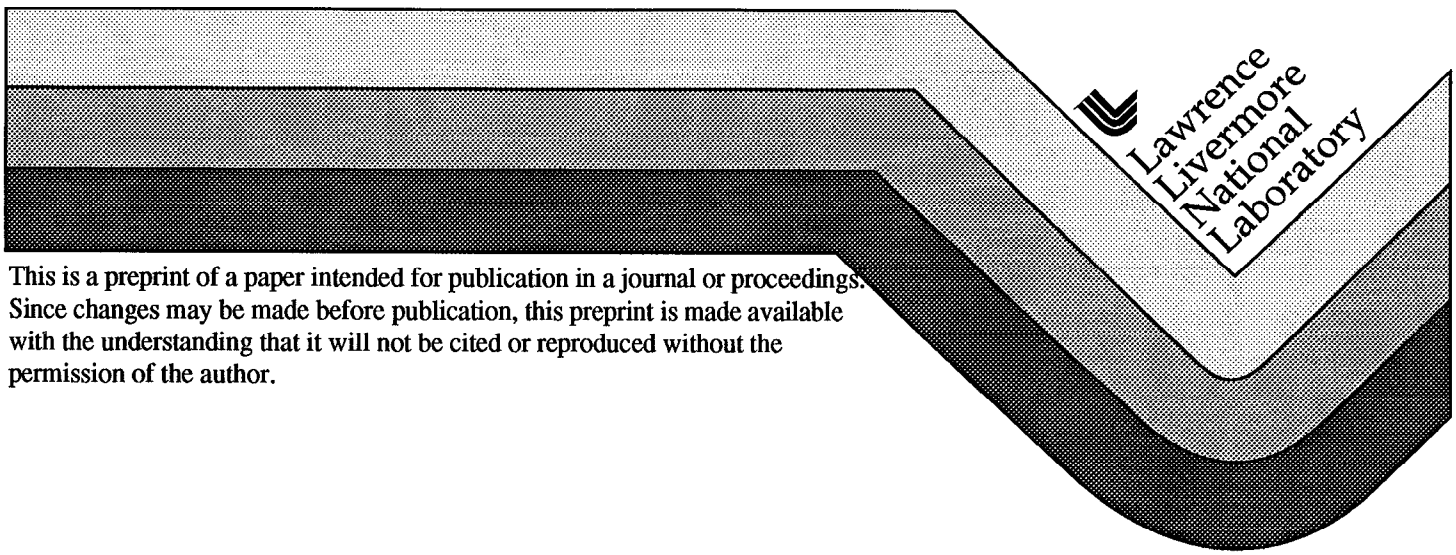

A Finite-Difference Frequency-Domain Code for Electromagnetic Induction Tomography

Nathan J. Champagne II, James G. Berryman, H. Michael Buettner,
J. Brian Grant, and Robert M. Sharpe
Lawrence Livermore National Laboratory,
P. O. Box 808, Livermore, CA 94551-9900

Abstract

We are developing a new 3D code for application to electromagnetic induction tomography and applications to environmental imaging problems. We have used the finite-difference frequency-domain formulation of Beilenhoff *et al.* (1992) and the anisotropic PML (perfectly matched layer) approach (Berenger, 1994) to specify boundary conditions following Wu *et al.* (1997). PML deals with the fact that the computations must be done in a finite domain even though the real problem is effectively of infinite extent. The resulting formulas for the forward solver reduce to a problem of the form Ax = y, where A is a non-Hermitian matrix with real values off the diagonal and complex values along its diagonal. The matrix A may be either symmetric or nonsymmetric depending on details of the boundary conditions chosen (*i.e.*, the particular PML used in the application). The basic equation must be solved for the vector x (which represents field quantities such as electric and magnetic fields) with the vector y determined by the boundary conditions and transmitter location. Of the many forward solvers that could be used for this system, relatively few have been thoroughly tested for the type of matrix encountered in our problem. Our studies of the stability characteristics of the Bi-CG algorithm raised questions about its reliability and uniform accuracy for this application. We have found the stability characteristics of Bi-CGSTAB [an alternative developed by van der Vorst (1992) for such problems] to be entirely adequate for our application, whereas the standard Bi-CG was quite inadequate. We have also done extensive validation of our code using semianalytical results as well as other codes. The new code is written in Fortran90 and is designed to be easily parallelized, but we have not yet tested this feature of the code. An adjoint method is being developed for solving the inverse problem for conductivity imaging (for mapping underground plumes), and this approach, when ready, will make repeated use of the current forward modeling code.

1 Introduction

Although electrical surveying techniques of both the current injection type and the magnetic field type have been well-known for many years (Telford *et al.*, 1976), efforts to turn these surveys into true 3D maps of subsurface physical properties have only been attempted in the last 10 to 20 years (Ramirez *et al.*, 1993; Tseng *et al.*, 1998). One of the reasons for this delay has been the necessity of large computer memories and fast computing machines, because it does not take a very large 3D forward modeling problem to swamp even today's most advanced computing capabilities. A recent review of the state of the art in 3D EM modeling (Zhdanov *et al.*, 1997) demonstrated the

limitations and lack of consensus on the best methods of computing EM fields in applications to inhomogeneous earth materials.

In this context, we are developing a new 3D code for application to electromagnetic induction tomography and applications to environmental imaging problems. We are using the finite-difference frequency-domain formulation of Beilenhoff *et al.* (1992) and the anisotropic PML (perfectly matched layer) approach (Berenger, 1994) to specify boundary conditions, following Wu *et al.* (1997). The present paper summarizes our progress to date on this code development.

2 Code Development

The goal of this code development effort is to produce an accurate and efficient forward simulation for EM fields that can then be easily used for inversion of ElectroMagnetic Induction Tomography (EMIT) field data. The FDFD (finite-difference frequency-domain) formulation presented here is an extension to lossy media of a method developed by Beilenhoff *et al.* (1992) for lossless media. The mesh truncation approach uses an anisotropic absorbing PML (perfectly matched layer) following the ideas of Berenger (1994) and Sacks *et al.* (1995). The absorbing regions have material parameters similar to those proposed by Kuzuoglu *et al.* (1996).

2.1 Finite-difference, frequency-domain formulation

To develop a system of equations to determine the electric and magnetic fields within a volume, the integral form of Maxwell's curl equations (Ampère's and Faraday's laws),

$$\oint_C \mathbf{H} \cdot d\ell = j\omega \int_S (\overline{\epsilon} \cdot \mathbf{E}) \cdot \hat{\mathbf{n}}\, dS + \int_S \mathbf{J} \cdot \hat{\mathbf{n}}\, dS \tag{1}$$

and

$$\oint_C \mathbf{E} \cdot d\ell = -j\omega \int_S (\overline{\mu} \cdot \mathbf{H}) \cdot \hat{\mathbf{n}}\, dS - \int_S \mathbf{M} \cdot \hat{\mathbf{n}}\, dS, \tag{2}$$

are used. Here $\mathbf{J}$ is the impressed electric current density, $\mathbf{M}$ is the impressed magnetic current density, both $\overline{\epsilon}$ and $\overline{\mu}$ are diagonal dyads, and C is the boundary of the open surface S. The integrals in (1) and (2) are applied to discrete elements (rectangular blocks) within the volume using the following equations:

$$\int_{-a/2}^{a/2} \mathbf{f} \cdot d\ell \rightarrow a f_m \tag{3}$$

and

$$\int_{-a/2}^{a/2} \int_{-b/2}^{b/2} \mathbf{f} \cdot \hat{\mathbf{n}}\, dS \rightarrow ab f_m, \tag{4}$$

where f_m is a center value associated with the mth cell shown in Figure 1. Note that the discrete electric field is located at the center of an edge and the discrete magnetic field flows through

Table 1: Cells surrounding the $m = \text{cell}(i, j, k)$ cell.

$d = \text{cell}(i-1, j, k)$	$u = \text{cell}(i+1, j, k)$
$l = \text{cell}(i, j-1, k)$	$r = \text{cell}(i, j+1, k)$
$f = \text{cell}(i, j, k-1)$	$b = \text{cell}(i, j, k+1)$

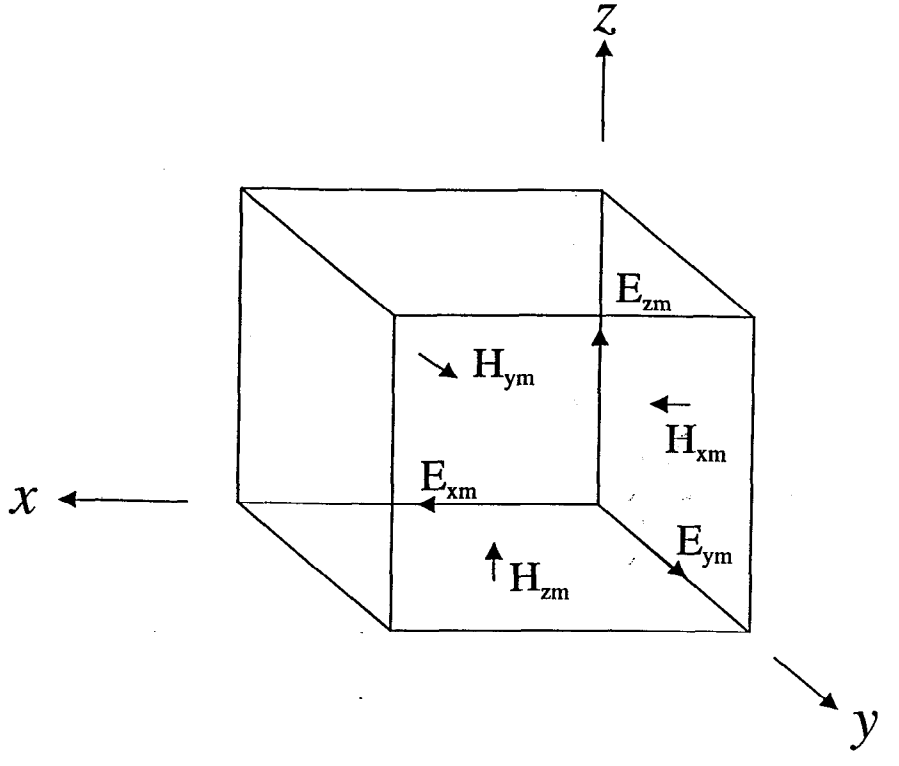

Figure 1: The field quantities associated with the mth cell (i,j,k).

the centroid of a face. Also, the mth cell is normally referred to as cell(i,j,k), but for notational convenience, a cell mapping using symbols such as u, d, l, r, f, b (for up, down, left, right, front, back) to specify the six cells surrounding the mth cell are used. This mapping is presented in Table 1. Cells other than the six cells adjacent to the six faces may also be labelled using the same mapping. For example, relative to cell m, cell df is cell$(i-1, j, k-1)$ and cell dlb is cell$(i-1, j-1, k+1)$.

The discretized form of (1) and (2) results in an equation for each field component. The resulting equations are cumbersome however, presenting each expression using matrices provides a compact form. Thus, using quantities discussed in the Appendix, (1) and (2) become

$$\boldsymbol{A}^T \boldsymbol{D}_{\tilde{\ell}}\, \vec{h} = j\omega\epsilon_0 \boldsymbol{D}_{A\epsilon}\, \vec{e} + \boldsymbol{D}_{\tilde{A}}\, \vec{j} \tag{5}$$

and

$$\boldsymbol{A}\boldsymbol{D}_{\ell}\, \vec{e} = -j\omega\mu_0 \boldsymbol{D}_A\, \boldsymbol{D}_{\mu}\, \vec{h} - \boldsymbol{D}_A\, \vec{m}, \tag{6}$$

respectively. The apparent lack of symmetry in the pair of equations (5) and (6) arises from the differences in method of discretizing ϵ and μ on the staggered grid (see the Appendix for the

details). Solving for the magnetic field (in order to eliminate it from the equations) in (6) and then substituting the result into (5) yields

$$\boldsymbol{A}^T \boldsymbol{D}_{\bar{\ell}} \boldsymbol{D}_{\mu}^{-1} \boldsymbol{D}_{\bar{A}}^{-1} \boldsymbol{A} \boldsymbol{D}_{\ell} \vec{e} - k_0^2 \boldsymbol{D}_{A\epsilon} \vec{e} = -j\omega\mu_0 \boldsymbol{D}_{\bar{A}} \vec{j} - \boldsymbol{A}^T \boldsymbol{D}_{\bar{\ell}} \boldsymbol{D}_{\mu}^{-1} \vec{m}, \tag{7}$$

which has a form quite analogous to that commonly used in finite element codes,

$$\nabla \times \left(\overline{\mu}_r^{-1} \cdot \nabla \times \mathbf{E} \right) - k_0^2 \overline{\epsilon}_r \cdot \mathbf{E} = -j\omega\mu_0 \mathbf{J} - \nabla \times \overline{\mu}_r^{-1} \cdot \mathbf{M}, \tag{8}$$

even though our goal here is to develop a finite difference code.

A commonly observed problem in numerical computations of Maxwell's equations arises due to a possible resonance at zero frequency. If this occurs, the resulting matrix has an eigenvalue at zero and therefore is not positive definite and not invertible. For the geometries considered here, the fields for resonant frequency of 0 Hz are generated only by electric charge within the volume. Such charges may develop as an artifact of numerical roundoff when evaluating the vector wave equation, especially at lower frequencies. This problem is avoided by eliminating any charge within the volume using a term analogous to

$$\nabla \left[\nabla \cdot (\overline{\epsilon}_r \cdot \mathbf{E}) \right] = \mathbf{0}. \tag{9}$$

This is achieved by starting from Gauss's law for the electric field in integral form,

$$\int_V \nabla \cdot (\overline{\epsilon}_r \cdot \mathbf{E}) \, dV = \oint_S (\overline{\epsilon}_r \cdot \mathbf{E}) \cdot \hat{\mathbf{n}} \, dS = 0, \tag{10}$$

to arrive at the discretized matrix expression

$$\left[\boldsymbol{D}_{\ell}^{-1} \boldsymbol{D}_{A\epsilon}^{*} \boldsymbol{B}^T \left(\boldsymbol{D}_{V\epsilon\epsilon}^{-1} \boldsymbol{B} \boldsymbol{D}_{A\epsilon} \right) \right] \vec{e} = \vec{0}, \tag{11}$$

where the matrices in parenthesis arise from discretizing (10) while the remaining matrices in the square bracket arise from discretizing (9) after the application of an integral identity. When (11) is added to (7), the result is

$$\left(\boldsymbol{A}^T \boldsymbol{D}_{\bar{\ell}} \boldsymbol{D}_{\mu}^{-1} \boldsymbol{D}_{\bar{A}}^{-1} \boldsymbol{A} \boldsymbol{D}_{\ell} - k_0^2 \boldsymbol{D}_{A\epsilon} + \boldsymbol{D}_{\ell}^{-1} \boldsymbol{D}_{A\epsilon}^{*} \boldsymbol{B}^T \boldsymbol{D}_{V\epsilon\epsilon}^{-1} \boldsymbol{B} \boldsymbol{D}_{A\epsilon} \right) \vec{e} = -j\omega\mu_0 \boldsymbol{D}_{\bar{A}} \vec{j} - \boldsymbol{A}^T \boldsymbol{D}_{\bar{\ell}} \boldsymbol{D}_{\mu}^{-1} \vec{m}. \tag{12}$$

However, a more symmetric form is obtained by multiplying through by $\boldsymbol{D}^{1/2}$ and then rewriting (12) as

$$\left(\boldsymbol{D}_{\ell}^{1/2} \boldsymbol{A}^T \boldsymbol{D}_{\bar{\ell}} \boldsymbol{D}_{\mu}^{-1} \boldsymbol{D}_{\bar{A}}^{-1} \boldsymbol{A} \boldsymbol{D}_{\ell}^{1/2} - k_0^2 \boldsymbol{D}_{A\epsilon} + \boldsymbol{D}_{\ell}^{-1/2} \boldsymbol{D}_{A\epsilon}^{*} \boldsymbol{B}^T \boldsymbol{D}_{V\epsilon\epsilon}^{-1} \boldsymbol{B} \boldsymbol{D}_{A\epsilon} \boldsymbol{D}_{\ell}^{-1/2} \right) \boldsymbol{D}_{\ell}^{1/2} \vec{e} = -j\omega\mu_0 \boldsymbol{D}_{\ell}^{1/2} \boldsymbol{D}_{\bar{A}} \vec{j} - \boldsymbol{D}_{\ell}^{1/2} \boldsymbol{A}^T \boldsymbol{D}_{\bar{\ell}} \boldsymbol{D}_{\mu}^{-1} \vec{m}. \tag{13}$$

2.2 PML formulation for mesh truncation

The mesh is truncated using perfectly matched layers (PML) that absorb electromagnetic waves following the general ideas of Berenger (1994). The PML is a representation of anisotropic media that satisfy

$$\mathbf{D} = \overline{\epsilon}_{\text{PML}} \cdot \mathbf{E} \qquad \text{and} \qquad \mathbf{B} = \overline{\mu}_{\text{PML}} \cdot \mathbf{H}, \tag{14}$$

where

$$\overline{\epsilon}_{\rm PML} = \overline{\epsilon} \cdot \overline{\Lambda} \qquad \text{and} \qquad \overline{\mu}_{\rm PML} = \overline{\mu} \cdot \overline{\Lambda}. \tag{15}$$

The symbol $\overline{\Lambda}$ stands for a diagonal dyad that has entries selected to absorb incident electromagnetic waves. The form of this dyadic quantity is determined by the normal to the PML interface. As an example, for a PML interface with a normal in the z direction, the form of $\overline{\Lambda}$ is given by Kuzuoglu and Mittra (1996) and by Wu *et al.* (1997) as

$$\overline{\Lambda}_z = \begin{bmatrix} a & 0 & 0 \\ 0 & a & 0 \\ 0 & 0 & 1/a \end{bmatrix}, \tag{16}$$

in which a is given by

$$a = 1 + \frac{f(x,y,z)}{1 + j\alpha\omega}, \tag{17}$$

where α is a constant and $f(x,y,z)$ is a function of position that falls to zero at the interface between the modeling space and the desired PML boundary. We have found through empirical studies that a suitable form for a is

$$a = 1 + \frac{f(x,y,z)}{1 + j\epsilon_0\omega}, \tag{18}$$

where $f(x,y,z)$ is given by

$$f(x,y,z) = \frac{(1-j)\beta}{\rho(x,y,z)}. \tag{19}$$

Here, $\rho(x,y,z)$ is the distance from the modeling space/PML interface to the cell of interest in the PML and β is chosen to determine the amplitude of $f(x,y,z)$.

3 Example

To demonstrate the accuracy of the new code (which we call FDFD for finite-difference/frequency-domain), we have tested various cases against results found in the literature. One example (see Figure 2) is for receivers down a borehole in a layered medium with air above the free surface, a 60m thick layer with conductivity = 0.3 S/m, a 25m thick layer with conductivity = 0.016 S/m, and a 60m layer with conductivity = 0.2 S/m at the bottom of the model, with appropriately designed PML absorbing layers on all six sides of the domain. Relative permittivity of all three earth layers is constant and assumed to equal 10.0. The frequency of the excitation is $f = 1$ kHz with the transmitter located at the free surface with an offset of 5m from the borehole. The finite difference representation was chosen so the unit spacing in the earth model was 2.5m, with 50 cells $\times$ 50 cells in the xy direction, and 10 layers of PML on all four sides. In the vertical direction, there were 68 cells in the earth model, 10 cells in the air above the free surface, and 10 more cells above and below for the PML layers. All PML cells are 10m thick in the directions away from the earth model. The overall problem is then approximately $70 \times 70 \times 100 \simeq 500,000$ cells. The computations were performed on a DEC Alpha 8400 Model 5/4400, and required approximately 2 hours of CPU time, including about 2000 iterations to achieve the desired convergence. This computation was serial and required about 500 MB of memory. In Figures 3 and 4 the results of the code calculations for the magnetic field magnitude and phase are compared to results for the same model obtained using the code EM1D (based on a semianalytical formula for such layered models) developed by Ki-Ha Lee at LBNL. The observed agreement is excellent.

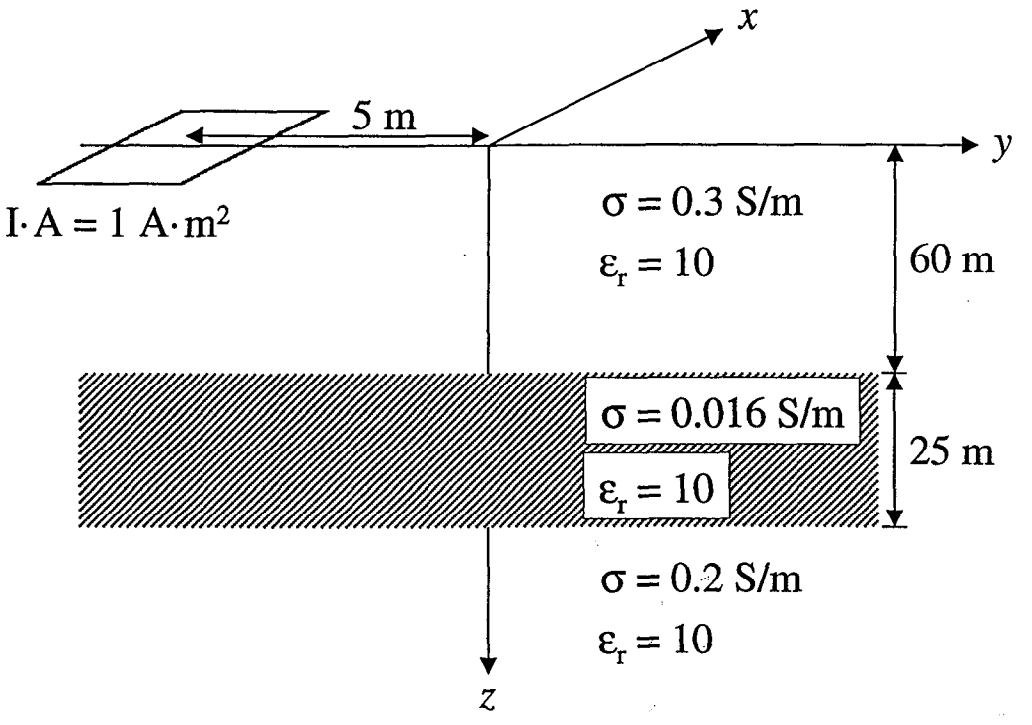

Figure 2: Current loop in a layered conducting medium.

4 Discussion

We continue to test and improve the EM forward modeling capability developed here. At the same time a new approach to the inverse problem of electromagnetics is being developed, in collaboration with Dr. Oliver Dorn and Prof. George Papanicolaou at Stanford University, based on the so-called "adjoint technique." This method has the very useful property that the inverse problem can be solved approximately by making two uses of the same forward modeling code we have already developed. Using a somewhat oversimplified description of our technique, the updates to the electrical conductivity will be obtained by first making one pass through the code using the latest best guess of the nature of the conducting medium, and then another pass with the adjoint operator (which for this problem is just the conjugate transpose of the forward modeling operator) applied to the differences in computed and measured data. Then the results of these two calculations are combined to determine updates to the original conductivity model. The resulting procedure is iterative and can be applied successively to parts of the data, *e.g.*, data associated with one transmitter location can be used to update the model before other transmitter locations are considered. This procedure has several of the same advantages as wave equation migration in reflection seismology (Claerbout, 1975) and is also related to recent methods in electromagnetics introduced by Zhdanov *et al.* (1996).

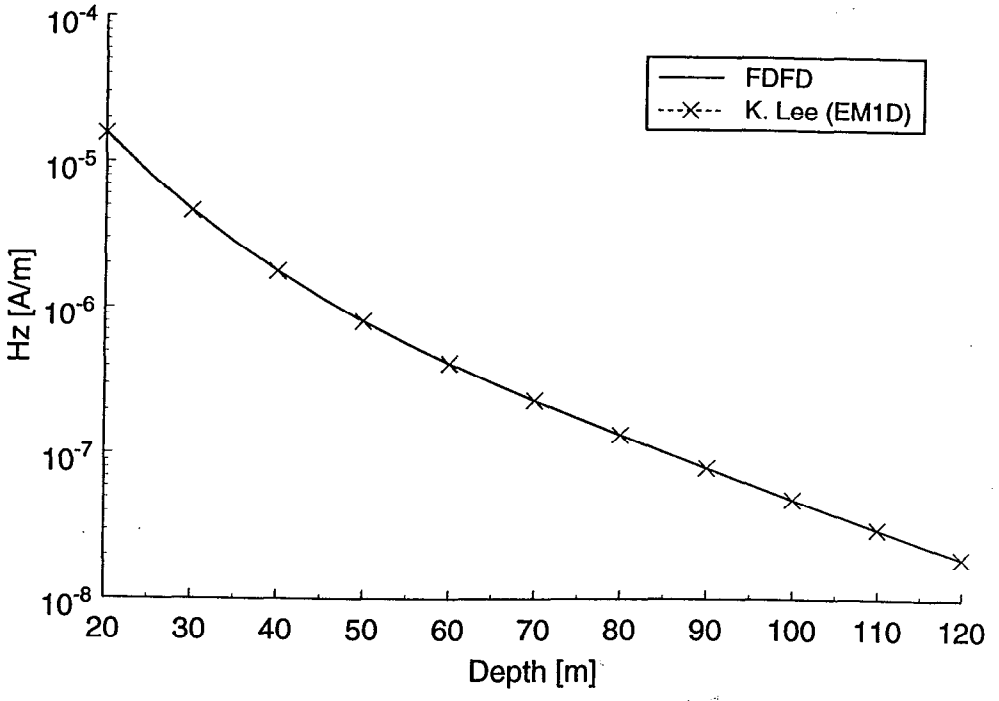

Figure 3: Comparison of FDFD computed magnitude of magnetic field in the layered model of Figure 2 with semianalytic results of Ki-Ha Lee (LBNL).

Acknowledgments

This work was performed under the auspices of the U.S. Department of Energy by the Lawrence Livermore National Laboratory under contract No. W-7405-ENG-48 and supported specifically by the Environmental Management Science Program of the Office of Environmental Management and the Office of Energy Research.

Appendix

Various special symbols used in this paper will now be defined. First, x_m, y_m, and z_m are the edge lengths of the mth cell (Figure 1) in the x, y, and z directions, respectively. Additional lengths associated with the magnetic fields (staggered grid cell lengths) are given by

$$\overline{x}_m = \frac{(x_m + x_d)}{2}, \qquad \overline{y}_m = \frac{(y_m + y_l)}{2}, \qquad \text{and} \qquad \overline{z}_m = \frac{(z_m + z_f)}{2}. \tag{20}$$

Then, the area of the staggered grid cell face is given by

$$a_{m_x} = \frac{y_m z_m + y_l z_l + y_f z_f + y_{lf} z_{lf}}{4}, \qquad a_{m_y} = \frac{x_m z_m + x_d z_d + x_f z_f + x_{df} z_{df}}{4}, \qquad \text{and}$$

$$a_{m_z} = \frac{x_m y_m + x_d y_d + x_l y_l + x_{dl} y_{dl}}{4} \tag{21}$$

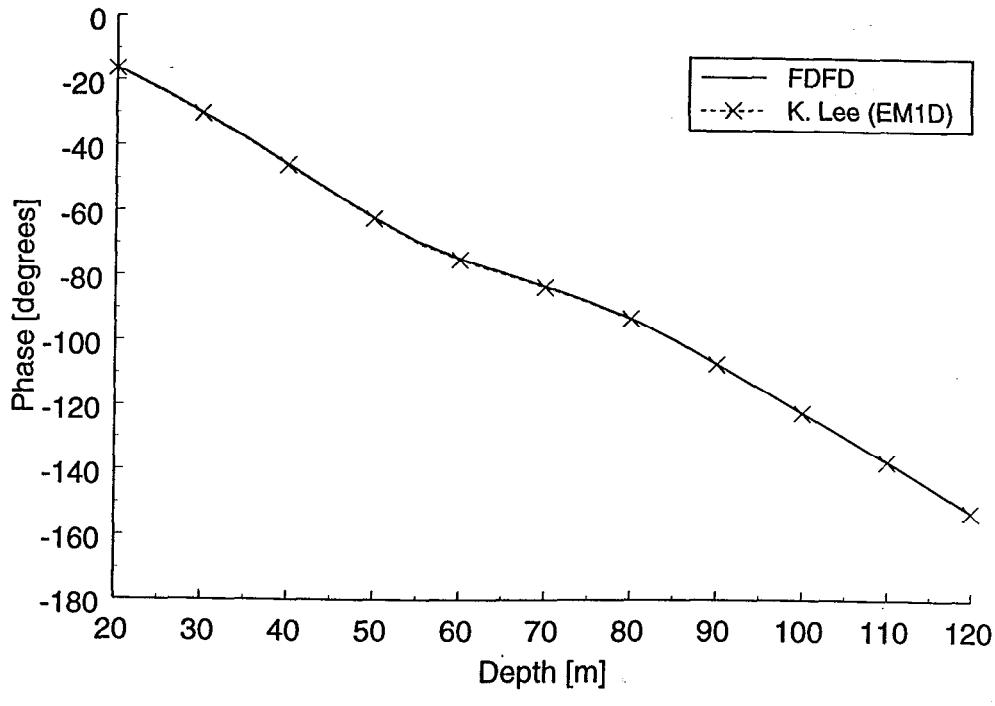

Figure 4: Comparison of FDFD computed phase of magnetic field in the layered model of Figure 2 with semianalytic results of Ki-Ha Lee (LBNL).

in the x, y, and z directions, respectively. Next, the permittivities associated with the electric field at an edge are given by

$$\overline{\epsilon}_{m_{xx}} = \frac{y_m z_m \epsilon_{m_{xx}} + y_l z_l \epsilon_{l_{xx}} + y_f z_f \epsilon_{f_{xx}} + y_{lf} z_{lf} \epsilon_{lf_{xx}}}{4}, \tag{22}$$

$$\overline{\epsilon}_{m_{yy}} = \frac{x_m z_m \epsilon_{m_{yy}} + x_d z_d \epsilon_{d_{yy}} + x_f z_f \epsilon_{f_{yy}} + x_{df} z_{df} \epsilon_{df_{yy}}}{4}, \tag{23}$$

and

$$\overline{\epsilon}_{m_{zz}} = \frac{x_m y_m \epsilon_{m_{zz}} + x_d y_d \epsilon_{d_{zz}} + x_l y_l \epsilon_{l_{zz}} + x_{dl} y_{dl} \epsilon_{dl_{zz}}}{4}. \tag{24}$$

And finally, the magnetic permeabilities associated with the magnetic field component at a face are given by

$$\overline{\mu}_{m_{xx}} = \frac{\mu_{m_{xx}} \mu_{d_{xx}} (x_m + x_d)}{(x_m \mu_{d_{xx}} + x_d \mu_{m_{xx}})}, \quad \overline{\mu}_{m_{yy}} = \frac{\mu_{m_{yy}} \mu_{l_{yy}} (y_m + y_l)}{(y_m \mu_{l_{yy}} + y_l \mu_{m_{yy}})}, \quad \overline{\mu}_{m_{zz}} = \frac{\mu_{m_{zz}} \mu_{f_{zz}} (z_m + z_f)}{(z_m \mu_{f_{zz}} + z_f \mu_{m_{zz}})}. \tag{25}$$

The set of all these cell quantities is represented using matrices as

$$\boldsymbol{D}_\ell = \mathrm{Diag}\left(\ldots, z_m, y_m, z_m, \ldots\right), \qquad \boldsymbol{D}_{\bar{\ell}} = \mathrm{Diag}\left(\ldots, \overline{z}_m, \overline{y}_m, \overline{x}_m, \ldots\right), \tag{26}$$

$$\boldsymbol{D}_A = \mathrm{Diag}\left(\ldots, x_m y_m, x_m z_m, y_m z_m, \ldots\right), \qquad \boldsymbol{D}_{\bar{A}} = \mathrm{Diag}\left(\ldots, a_{m_z}, a_{m_y}, a_{m_x}, \ldots\right), \tag{27}$$

$$\boldsymbol{D}_{A\epsilon} = \mathrm{Diag}\left(\ldots, \overline{\epsilon}_{m_{zz}}, \overline{\epsilon}_{m_{yy}}, \overline{\epsilon}_{m_{xx}}, \ldots\right), \quad \text{and} \quad \boldsymbol{D}_{\mu} = \mathrm{Diag}\left(\ldots, \overline{\mu}_{m_{zz}}, \overline{\mu}_{m_{yy}}, \overline{\mu}_{m_{xx}}, \ldots\right). \tag{28}$$

Additionally, the volume matrix is given by

$$\boldsymbol{D}_{V\epsilon\epsilon} = \mathrm{Diag}\left(\ldots, V_{m_z}, V_{m_y}, V_{m_x}, \ldots\right), \tag{29}$$

where

$$\begin{aligned} V_{m_\alpha} = \frac{1}{8}\Big[&|\epsilon_{m_{\alpha\alpha}}|^2 x_m y_m z_m + |\epsilon_{d_{\alpha\alpha}}|^2 x_d y_d z_d + |\epsilon_{l_{\alpha\alpha}}|^2 x_l y_l z_l + |\epsilon_{f_{\alpha\alpha}}|^2 x_f y_f z_f + \\ &|\epsilon_{df_{\alpha\alpha}}|^2 x_{df} y_{df} z_{df} + |\epsilon_{dl_{\alpha\alpha}}|^2 x_{dl} y_{dl} z_{dl} + |\epsilon_{lf_{\alpha\alpha}}|^2 x_{lf} y_{lf} z_{lf} + |\epsilon_{dlf_{\alpha\alpha}}|^2 x_{dlf} y_{dlf} z_{dlf}\Big]. \end{aligned} \tag{30}$$

The vectors $\vec{e}$, $\vec{h}$, $\vec{j}$, and $\vec{m}$ have the general form

$$\vec{f} = \left(\ldots, F_{m_z}, F_{m_y}, F_{m_x}, \ldots\right). \tag{31}$$

Finally, the coefficient matrices $\boldsymbol{A}$ and $\boldsymbol{B}$ are given by (note that the first row displayed in each of the two following equations is shown to clarify the indexing scheme used in the matrix shown)

$$\boldsymbol{A} = \begin{array}{c} \begin{array}{cccccccccccccccc} \cdots & z_m & y_m & x_m & z_u & y_u & x_u & \cdots & z_r & y_r & x_r & \cdots & z_b & y_b & x_b & \cdots \end{array} \\ \left[\begin{array}{cccccccccccccccc} \ddots & & & & & & & & & & & & & & & \\ & 0 & -1 & 1 & 0 & 1 & 0 & \cdots & 0 & 0 & -1 & \cdots & 0 & 0 & 0 & \\ & 1 & 0 & -1 & -1 & 0 & 0 & \cdots & 0 & 0 & 0 & \cdots & 0 & 0 & 1 & \\ & -1 & 1 & 0 & 0 & 0 & 0 & \cdots & 1 & 0 & 0 & \cdots & 0 & -1 & 0 & \\ & & & & \ddots & & & & & & & & & & & \end{array}\right] \end{array} \tag{32}$$

and

$$\boldsymbol{B} = \begin{array}{c} \begin{array}{cccccccccccc} \cdots & z_f & \cdots & y_l & \cdots & x_d & z_m & y_m & x_m & \cdots \end{array} \\ \left[\begin{array}{cccccccccccc} \ddots & & & & & & & & & & & \\ & 1 & & & & & & & & & & \\ & & \ddots & & & & & & & & & \\ & & & 1 & & & & & & & & \\ & & & & \ddots & & & & & & & \\ & & & & & 1 & & & & & & \\ & -1 & \cdots & -1 & \cdots & -1 & 1 & 1 & 1 & & & \\ & -1 & \cdots & -1 & \cdots & -1 & 1 & 1 & 1 & & & \\ & -1 & \cdots & -1 & \cdots & -1 & 1 & 1 & 1 & & & \\ & & & & & & & & & \ddots & & \end{array}\right] \end{array}. \tag{33}$$

References

Beilenhoff, K., W. Heinrich, and H. L. Hartnagel, "Improved finite-difference formulation in frequency domain for three-dimensional scattering problems," *IEEE Trans. Microwave Theory Tech.* **40**, 540–546, 1992.

Berenger, J. P., "A perfectly matched layer for the absorption of electromagnetic waves," *J. Computational Phys.* **114**, 185–200, 1994.

Berryman, J. G., "Challenges for computational physics in underground imaging of electrically conducting contaminant plumes," invited talk P2.03 in special session on Geological Phenomena at the *International Conference on Computational Physics*, American Physical Society, Division of Computational Physics, Santa Cruz, California, August 25–29, 1997.

Buettner, H. M., and J. G. Berryman, "An electromagnetic induction tomography field experiment at Lost Hills, CA," SAGEEP, Oakland Marriott Center, Oakland, California, March 14–18, 1999.

Claerbout, J. F., *Fundamentals of Geophysical Data PRocessing: With Applications to Petroleum Prospecting*, McGraw-Hill, New York, 1976.

Kuzuoglu, M., and R. Mittra, "Frequency dependence of the constitutive parameters of causal perfectly matched anisotropic absorbers," *IEEE Microwave Guided Wave Lett.* **6**, 447–449, 1996.

Ramirez, A., W. D. Daily, D. LaBrecque, E. Owen, and D. Chesnut, Monitoring an underground steam injection process using electrical resistance tomography, *Water Resources Res. 29*, 73–87, 1993.

Telford, W. M., L. P. Geldart, R. E. Sheriff, and D. A. Keys, *Applied Geophysics*, Cambridge University Press, Cambridge, England, 1976, Section 3.5.4. Sacks, Z. S., D. M. Kingsland, R. Lee, and J. F. Lee, A perfectly matched anisotropic absorber for use as an absorbing boundary condition, *IEEE Trans. Antennas Prop.* **43**, 1460–1463, 1995.

Torres-Verdin, C., and T. M. Habashy, "Rapid 2.5-dimensional forward modeling and inversion via a new nonlinear scattering approximation," *Radio Sci.* **29**, 1051–1079, 1994. Tseng, H.-W., A. Becker, M. J. Wilt, and M. Deszcz-Pan, "A borehole-to-surface electromagnetic survey," *Geophysics* **73**, 1565–1572, 1998.

van der Vorst, H. A., "Bi-CGSTAB: A fast and smoothly converging variant of Bi-CG for the solution of non-symmetric linear systems," *SIAM J. Sci. Stat. Comput.* **12**, 631–644, 1992.

Wu, J. Y., D. M. Kingsland, J. F. Lee, R. Lee, "A comparison of anisotropic PML to Berenger's PML and its application to the finite-element method for EM scattering," *IEEE Trans. Antennas Propagat.* **45**, 40–50, 1997.

Zhdanov, M. S., and S. Feng, "Quasi-linear approximation in 3D electromagnetic modeling," *Geophysics* **61**, 646–665, 1996.

Zhdanov, M. S., P. Traynin, and J. R. Booker, "Underground imaging by frequency-domain electromagentic migration," *Geophysics* **61**, 666–682, 1996.

Zhdanov, M. S., I. M. Varentsov, J. T. Weaver, N. G. Golubev, and V. A. Krylov, "Methods for modeling electromagnetic fields: Results from COMMEMI — The international project on the Comparison Of Modeling Methods for ElectroMagnetic Induction," *J. Appl. Geophys.* **37**, 133–271, 1997.